Bioorganic Chemistry 93 (2019) 103269

Contents lists available at ScienceDirect

Bioorganic Chemistry

journal homepage: www.elsevier.com/locate/bioorg

A structure-activity relationship study of Forkhead Domain Inhibitors (FDI): The importance of halogen binding interactions

Seyed Amirhossein Tabatabaei Dakhili, David J. Pérez, Keshav Gopal, Seyed Yasin Tabatabaei Dakhili, John R. Ussher, Carlos A. Velázquez-Martínez*

Faculty of Pharmacy and Pharmaceutical Sciences, University of Alberta, Edmonton, AB, Canada

ARTICLE INFO

Keywords:
FOXM1
FDI-6
Direct FOXM1 inhibitors
Transcription factor

ABSTRACT

The Forkhead boX M1 (FOXM1) protein is an essential transcription factor required for the normal activation of human cell cycle. However, increasing evidence supports a correlation between FOXM1 overexpression and the onset of several types of cancer. Based on a previously reported molecular modeling and molecular dynamics simulations (MD) study, we hypothesized the role of an essential halogen-bonding interaction between the 4-fluorophenyl group in the forkhead domain inhibitor-6 (FDI-6) and an Arg297 residue inside the FOXM1-DNA binding domain (DBD). To prove the importance of this binding interaction, we synthesized and screened ten FDI-6 derivatives possessing different groups at the 4-fluorophenyl position of the lead molecule. Briefly, we found that derivatives possessing a 4-chlorophenyl, 4-bromophenyl, or a 4-iodophenyl group, were equipotent to the original 4-fluorophenyl moiety present in FDI-6, whereas derivatives without this 4-halogen moiety were inactive. We also observed that positional isomers in which the halogen was relocated to positions 2- or 3- on the phenyl group were significantly less active. These results provide evidence to support the essential role of a 4-halophenyl bonding interaction, with the Arg297 residue in the FOXM1-DBD, to exert inhibition of transcriptional activity.

1. Introduction

The Forkhead Box M1 (FOXM1) protein is an essential transcription factor required for mitotic progression and cell division. Unlike normal cells, cancer cells (of practically any tissue origin) undergo changes leading to overexpression of FOXM1 and the abnormal activation of its transcriptional cascade [1–3]. Hence, cancer cells sustain a rapid cell replication pattern. In addition to its role in cell proliferation, FOXM1 is also involved in cancer initiation [4,5], angiogenesis [6,7], and metastasis [8]. Fig. 1 presents a schematic summary of the different roles played by FOXM1 in cancer initiation and cancer progression. The carcinogenic features associated with an overexpression of FOXM1 make this protein an emerging and promising drug target for cancer treatment [9,10].

Similar to other FOX proteins, FOXM1 has a conserved DNA Binding Domain (DBD) that is responsible for binding to the corresponding promoter regions [11]. Hypothetically, any small molecule capable of binding to this winged helix could inhibit the FOXM1/DNA complex. Nevertheless, transcription factors have been regarded as “challenging” or “inaccessible” using small molecules [12]. This generalization was, at least in part, due to the large solvent-accessible area observed on the transcription factor and the lack of well-defined binding pockets on the protein’s hydrophobic surface [13,14]. In this regard, Gormally et al. [14] reported a high-throughput screening technique to test more than 50,000 small-molecules, selecting those capable of inhibiting the binding interaction between FOXM1 and its DBD. Gormaly’s group selected 16 different Forkhead Domain Inhibitors (abbreviated as “FDI”), among which, the compound FDI-6 was the most potent and selective.

Abbreviations: FOXM1, forkhead box M1; MD, molecular dynamics; MTT, 3-(4,5-dimethylthiazol-2-yl)-2,5-diphenyltetrazolium bromide; EMSA, Electrophoretic Mobility Shift Assay; DBD, DNA binding domain; SEM, standard error of the mean; ANOVA, analysis of variance; TLC, thin layer chromatography; FDI, forkhead domain inhibitor; NMR, nuclear magnetic resonance; DMSO, dimethyl sulfoxide; TMS, tetramehtylsilane; ATCC, American type culture collection; DMEM, Dulbecco's Modified Eagle's Medium; RMPI, Roswell Park Memorial Institute medium; FBS, foetal bovine serum; SDS-PAGE, sodium dodecyl sulfate- polyacrylamide gel electrophoresis; LB, luria broth; IPTG, Isopropyl β-D-1-thiogalactopyranoside; GST, glutathione s-transferase; dsDNA, double stranded DNA; RT, room temperature; EDTA, Ethylenediaminetetraacetic acid; DTT, Dithiothreitol; K_d, dissociation constant; K_i, inhibition constant; PDB, protein data bank; RMSD, root mean square fluctuation; MMPBSA, molecular mechanic poisson boltzmann surface area; VDW, van der waals

* Corresponding author.
E-mail address: velazque@ualberta.ca (C.A. Velázquez-Martínez).

https://doi.org/10.1016/j.bioorg.2019.103269
Received 22 March 2019; Received in revised form 8 August 2019; Accepted 9 September 2019
Available online 12 September 2019
0045-2068/

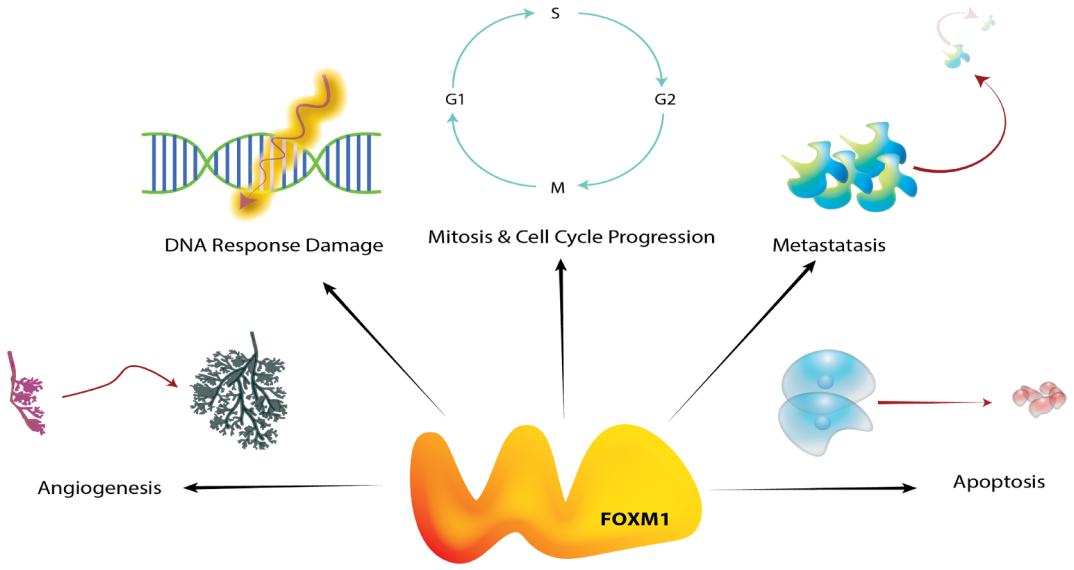

Fig. 1. The role of FOXM1 in cancer initiation and cancer progression. FOXM1 is involved in the activation of different genes and the expression of proteins that control angiogenesis, DNA repair, metastasis, and apoptosis.

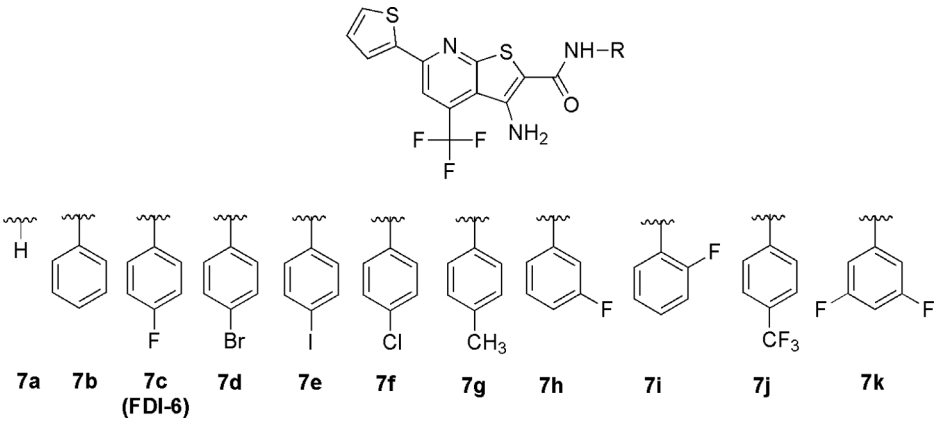

Fig. 2. Compounds **7a-7k** were prepared by replacing the 4-fluorophenyl group of FDI-6 (**7c**).

We previously conducted and reported a detailed in silico study [15] to determine FOXM1-DBD/DNA binding interactions exerted by three structurally-different FOXM1 inhibitors, namely thiostrepton [16,17], troglitazone [18], and FDI-6 [14]. In our previous study we proposed a protein-drug-DNA binding model involving a sulfur-His287 interaction. In addition, we also proposed another essential drug binding interaction involving the fluorine atom at the 4-position of the phenyl ring present in FDI-6, and the Arg297 residue in FOXM1. To prove the importance of this halogen binding, in this complementary study we report (i) a Structure-Activity Relationship (SAR) between the parent (lead) drug FDI-6, and ten derivatives possessing halogen (Cl, Br, I) atoms, as well as other substituents at the 4-fluorophenyl (H-, CH_3-, CF_3-) position. Furthermore, we also studied the effects of relocating the 4-fluorine atom to a 2- and 3-position (Fig. 2).

We report preliminary evidence validating the essential role of a halogen atom in FDI-6 derivatives, responsible for binding to an Arg297 residue. The results of our experiments validate the hypothesis of a 4-(halo)phenyl moiety as an essential structural feature in FDIs, as one of the required drug binding forces at the interface of the FOXM1 protein and its DBD.

2. Results and discussion

2.1. Design and synthesis

To conduct a structure-activity relationship study on the role of the 4-fluorine atom present in FDI-6, we synthesized ten derivatives possessing different functional groups at the 4-position of a phenyl group present in the lead molecule. We adapted the methods previously reported for the synthesis of FDI-6 [14,19] and prepared derivatives **7a-7k**, with overall yields around 80%, using a microwave-assisted synthesis. The proposed series of test molecules include FDIs devoid of the 4-fluorophenyl group (**7a**); replacement of the 4-fluorophenyl by a simple Ph moiety (**7b**); 4-bromophenyl (**7d**), 4-iodophenyl (**7e**); 4-chlorophenyl (**7f**); 4-methylphenyl (**7g**); 3-fluorophenyl (**7h**); 2-fluorophenyl (**7i**); 3,5-difluorophenyl (**7k**); and a 4-trifluoromethylphenyl, **7j**) (Scheme 1).

2.2. Cell proliferation inhibition assay

First, we determined the effect exerted by FDI-derivatives **7a-7k** on cancer cell proliferation using two human breast cancer cell lines, namely the triple negative-breast cancer cell line MDA-MB-231, and the estrogen receptor positive cell line MCF-7, using the MTT assay. Briefly, after a 72 h-incubation period of the corresponding cell line with the

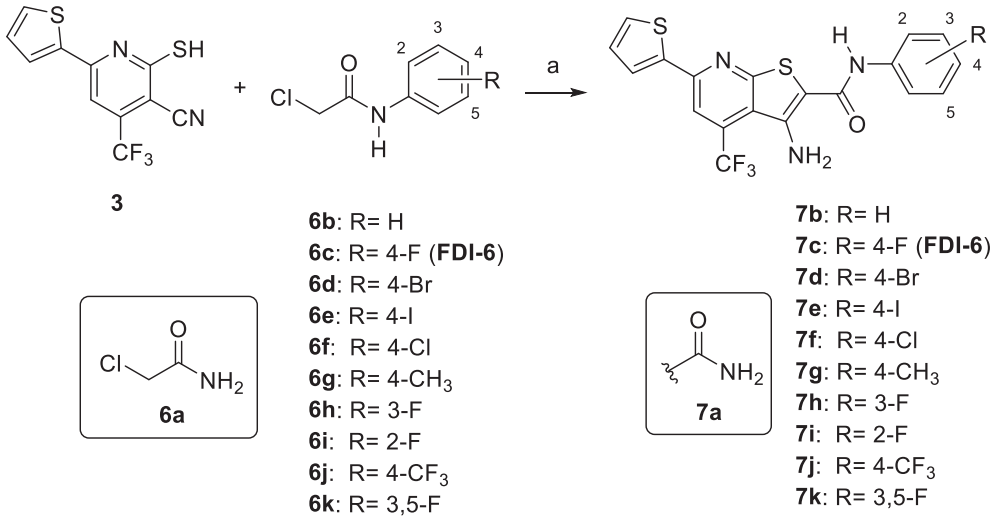

Scheme 1. Chemical synthesis of FDI-6 derivatives, **7a**-**7k**. [a]Reagents and conditions: K_2CO_3, EtOH, 90 °C, μW, 2 h.

Table 1
IC_{50} values determined for test molecules using the human breast cancer cell lines MDA-MB-231 and MCF-7; these values were calculated after a 72 h-incubation period with the drug molecules; all values represent the mean ± SEM of three different experiments, each one in triplicate.

Compound	MDA-MB-231 IC_{50} (μM)	MCF-7 IC_{50} (μM)
7a	> 50	> 50
7b	> 50	35.27 ± 6.03
7c (FDI-6)	31.1 ± 8.7	13.43 ± 1.82
7d	12.5 ± 4.4	3.04 ± 0.75
7e	9.8 ± 2.2	1.36 ± 0.39
7f	14.6 ± 4.2	2.90 ± 1.15
7g	24.8 ± 5.0	11.25 ± 2.9
7h	35.75 ± 6.3	23.35 ± 6.09
7i	> 50	> 50
7j	12.6 ± 1.6	10.53 ± 1.9
7k	> 50	> 50

test molecules (at increasing concentrations), we observed that drug potency was significantly reduced for molecules without a 4-(halo) phenyl group (**7a**, **7b**), as well as for drug **7i** in which the fluorine atom was changed from the 4- to the 2-position; this was also observed for drug **7k** possessing a 3,5-difluorophenyl moiety. Interestingly, replacement of the fluorine atom present in FDI-6 (**7c**) by a 4-bromo (**7d**), 4-iodo (**7e**), or 4-chloro (**7f**) resulted in increased potency (decreased cell proliferation) in both cell lines. However, the MCF-7 cancer cell line was more susceptible to proliferation inhibition by the drug molecules. Interestingly, there was an apparent inverse correlation between the electronegativity of the halogen atom and the potency of the corresponding derivative, in which the lower the electronegativity of the halogen atom, the higher the potency (Table 1). Overall, these results suggest that the 4-(halo)phenyl ring is essential for cancer cell proliferation inhibition in vitro.

Assuming that a methyl group could be a suitable bioisosteric replacement for some halogen atoms [20], we synthesized and screened compounds **7g** [4-(CH_3) phenyl] and **7j** [4-(CF_3)phenyl]. In this regard, we observed an equipotent potency for both drugs compared to the analogs possessing a 4-(halo)phenyl group, including the lead drug FDI-6. Consequently, these observations strongly suggest that the 4-substituted phenyl ring in FDI is essential to exert significant cell proliferation inhibition of these two breast cancer cell lines.

We also investigated the effect produced by moving the fluorine atom from the 4- to 3- position (compound **7h**) and we observed a minor decrease in potency compared to the lead molecule, which in addition to the observation that the 2-fluorophenyl compound was inactive (up to a maximum test drug concentration of 50 μM), we propose that the halogen-Arg297 binding interaction becomes weaker as the halogen is relocated farther away from the initial 4-position. This statement is based on the assumption that the observed cell proliferation inhibition exerted by the drugs is, at least in part, FOXM1-dependent. Finally, we observed that the compound having a 3,5-difluorophenyl moiety (**7k**) was inactive, likely not because of weaker binding interactions, but because it was not soluble enough in the cell media employed in the MTT assay (we observed precipitation at increasingly higher concentrations). Nevertheless, we will need to carry out additional experiments using different pharmaceutical excipients (other than DMSO) to increase the water solubility of this compound.

2.3. FOXM1 expression (western blot)

Considering that FOXM1 modulates its own transcriptional expression [21] we determined the effect exerted by the test drugs on the expression levels of this protein, by western blot analysis (whole cell lysis), after a 24 h-incubation period with the corresponding drug molecules, in triple negative-breast cancer cells (MDA-MB-231). We conducted this experiment assuming that a drug-dependent decrease in FOXM1 at the protein level could be due, at least in part, due to a drug-induced dissociation of the nuclear FOXM1-DNA complex, which in turn would suggest transcriptional inhibition. We observed a drug-dependent decrease in FOXM1 protein expression in MDA-MB-231 breast cancer cells (Fig. 3). Based on a simple structure-activity relationship study, we can make a few preliminary statements describing the effect of substituting specific functional groups on protein expression in these cells. For example, compound **7a** (devoid of the 4-fluorophenyl group present in the lead drug FDI-6) and compound **7b** [possessing a simpler 4-(phenyl) moiety], were practically inactive at 40 μM. As expected, the lead molecule FDI-6 [4-(fluoro)phenyl; **7c**] significantly decreased the expression of FOXM1. Interestingly, compounds possessing a 4-(bromo) phenyl (**7d**), 4-(iodo)phenyl (**7e**) and 4-(chloro)phenyl (**7f**) were equipotent to FDI-6 (non-significant differences between them) in this assay, correlating well with the cancer cell proliferation inhibition assay. Nevertheless, we observed that compound **7g** [4-(methyl) phenyl] did not exert a significant decrease in FOXM1 expression despite its good cell proliferation inhibitory profile. This suggests that bioisosteric replacement with a methyl group may not be a suitable approach to decrease the expression of FOXM1 in triple negative-breast cancer cells. Finally, extending the SAR study to other derivatives in the series, we observed that compound **7h** [3-(fluoro)phenyl] was active at

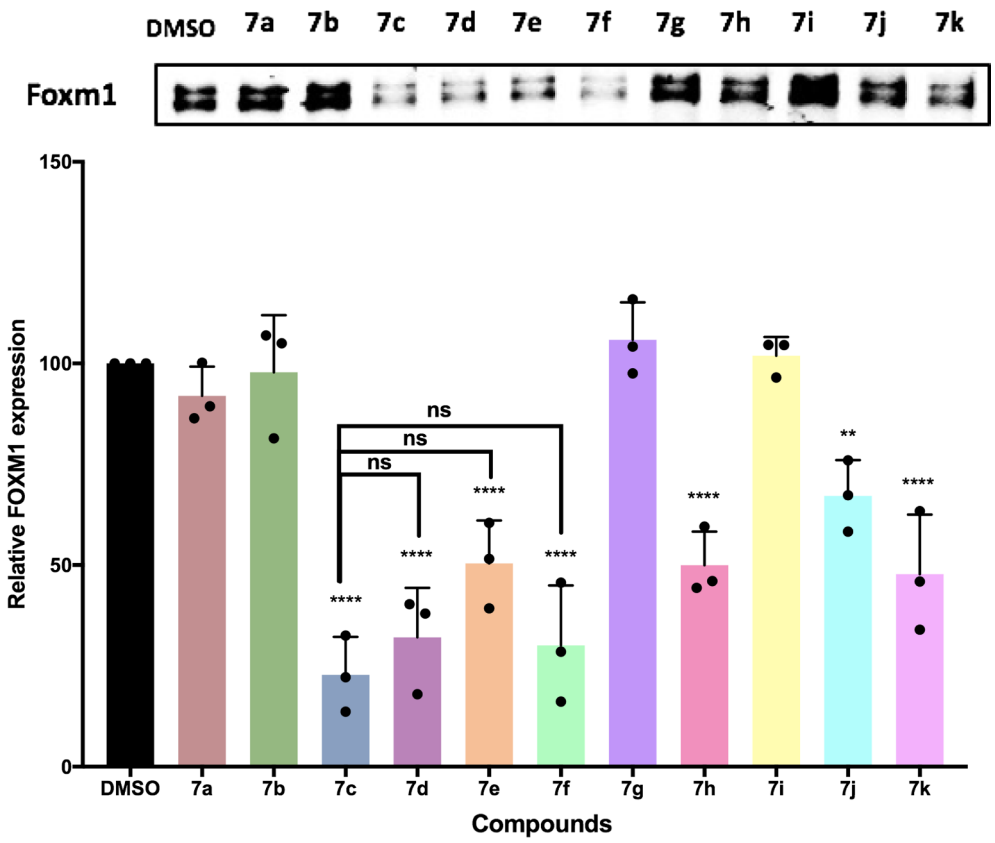

Fig. 3. Expression levels of the FOXM1 protein and the concentration-dependent inhibitory effect produced by the test drugs; incubation time: 24 h; cell line: triple negative-breast cancer (MDA-MB-231); drug concentration = 40 μM; the bars represent the corresponding average values obtained after carrying out three independent experiments ± SEM; one-way ANOVA was used to determine significance (* = $P \leq 0.05$, ** = $P \leq 0.01$, **** = $P \leq 0.0001$) compared to DMSO.

40 μM, but compound **7i** [2-(fluoro)phenyl] was inactive, and this observation provides a "fine-tuning" of the hypothesis described above in the sense that, the farther apart from position 4-, the weaker the binding interaction. We observed that compound **7k** (3,5-difluorophenyl) and **7j** [4-(trifluoromethyl)phenyl] exerted only a moderate decrease in FOXM1 expression levels, likely due to low water solubility.

These results are in accordance with our hypothesis highlighting the role of a 4-(halo)phenyl moiety for the drug binding process resulting in inhibition of FOXM1's transcriptional activity. The results obtained in the western blot assay support the assumption that drugs possessing the 4-(halo)phenyl moieties decrease the expression of FOXM1 in breast cancer cells, and provide evidence in favor of a 4-(halo)phenyl group/Arg297 binding interaction in the FOXM1 protein.

2.4. Electrophoretic Mobility Shift Assay (EMSA)

This cell-free assay was selected based on its ability to measure the concentration-dependent effect produced by drug molecules on the FOXM1-DNA complex in vitro. This screening method was first reported by Gormally et al. [14] as part of a high-throughput screening approach to find new FOXM1 inhibitors, in which the drug FDI-6 was identified as the most potent molecule. Based on their model, we incubated the recombinant FOXM1-DBD reported to bind to DNA (also called FOXM1-DNA binding domain, or FOXM1-DBD), with the target DNA, in the presence of the corresponding FDI derivatives, and then running the mixture on native polyacrylamide gel. As shown in Fig. 4, we observed that compounds **7a** (devoid of the 4-(halo)phenyl group) and **7b** (having a simple phenyl) were weak drugs (IC_{50} values = 128.2 and 121.7 μM respectively), whereas compounds **7c** [4-(fluoro)phenyl], **7d** [4-(bromo)phenyl], and **7e** [4-(iodo)phenyl] were significantly more active (IC_{50} values around 40 μM). Compound **7f** [4-(chloro)phenyl], the most active molecule in this series (IC_{50} value = 27.2 μM), was about 2-fold more potent than the lead drug FDI-6. These observations provide one more piece of evidence confirming our initial hypothesis, in which we proposed the need for a 4-halo substituted phenyl ring in the FDI scaffold.

Compound **7g** possessing a 4-CH_3 bioisosteric replacement was much less active (IC_{50} = 228.9 μM) than **7c** (FDI-6) and compared to other halogen-containing derivatives. Nevertheless, we observed that a 4-(trifluoromethyl)phenyl group (**7j**) exerted higher activity (IC_{50} = 27.5 μM), supporting the need of having a halogen atom at the 4-phenyl position, essential to exert a binding interaction with Arg297 in FOXM1. Finally, moving the fluorine atom from the 4-position (**7c**) to 3-position (**7h**) did not decrease the activity (IC_{50} = 42.6 μM), but when the halogen is farther away (2-position; **7i**) the potency decreased (IC_{50} = 69.6 μM).

Finally, when we screened compounds **7j** and **7k**, possessing a [4-(trifluoromethyl)phenyl] and a 3,5-(difluoro)phenyl moiety, respectively, we observed a good inhibitory profile of the FOXM1-DNA complex (IC_{50} = 27.6 and 27.5 μM respectively). It should be noted that in contrast to the results obtained in the protein immunoblot assay described previously, in which compound **7j** and **7k** were relatively weak, in the cell-free EMSA assay the binding interactions exerted by these molecules may be more significant (cell membrane permeability is not required). Considering that the soluble fraction of the drug is in direct contact with the FOXM1 protein, it is possible that this is good enough to exert inhibition of the FOXM1/DNA complex. This observation should be considered when trying to extrapolate results from one assay to the other, and therefore, to assess the complete profile of any given drug molecule as a transcription factor "inhibitor", one must consider the results from several screening assays. Moreover, to compare the activity of different inhibitors, the Ki values (Fig. 4) should be used as a complementary evaluation parameter, because IC_{50} values can be altered by changing the protein concentration and, hence, could be misleading.

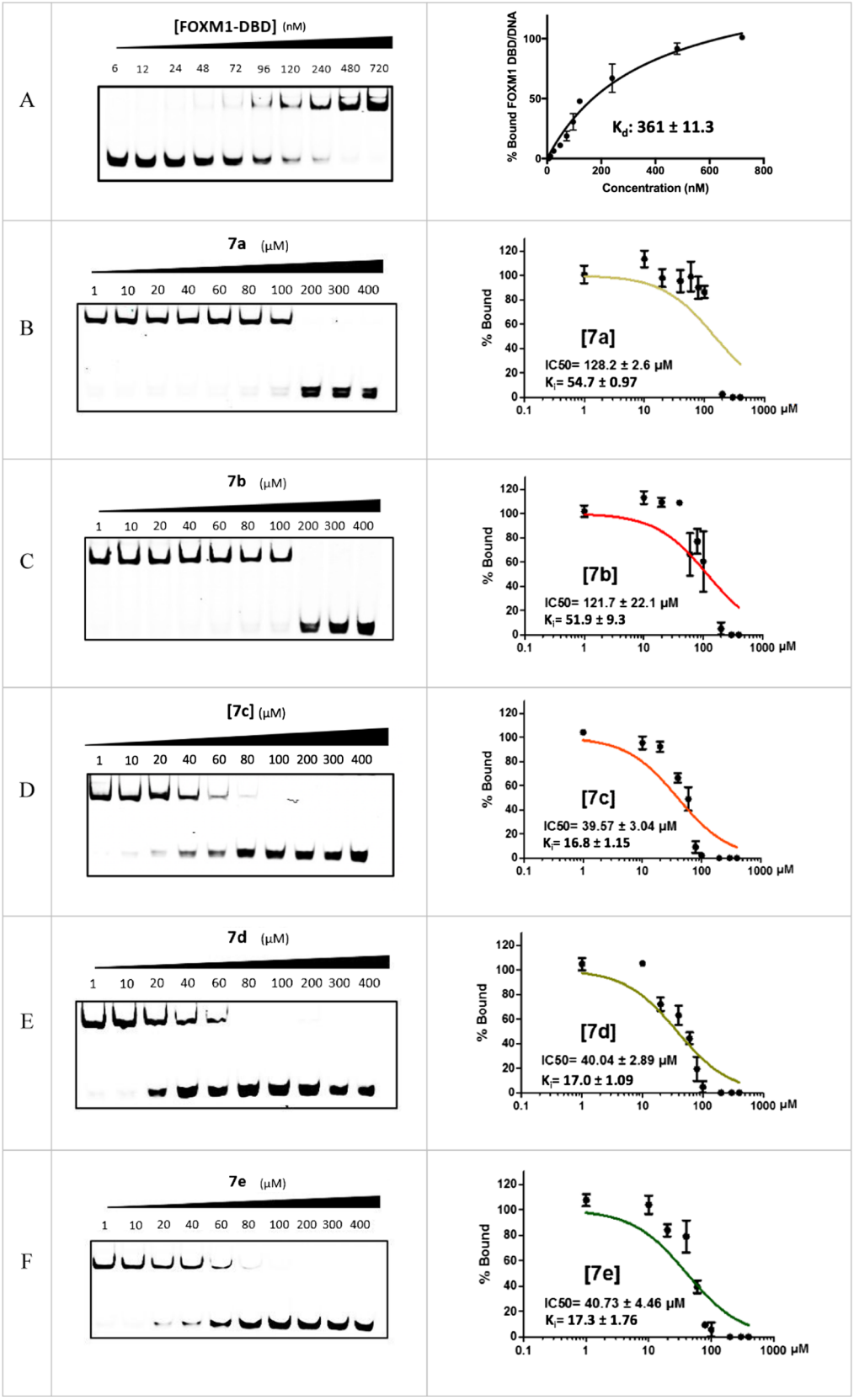

Fig. 4. Electrophoretic Mobility Shift Assay. (A) Titration curve of FOXM1-DBD protein with the target DNA (5-/IRD700/-AAACAAACAAACAATCAAACAAAC AAACAATC-3′); (**B** to **L)** concentration-dependent effects of the drug molecules on the FOXM1-DNA complex presenting the calculated IC_{50} values, and their corresponding Ki's; all data are reported as average of three replicates (n = 3) and the error bars represent the SEM.

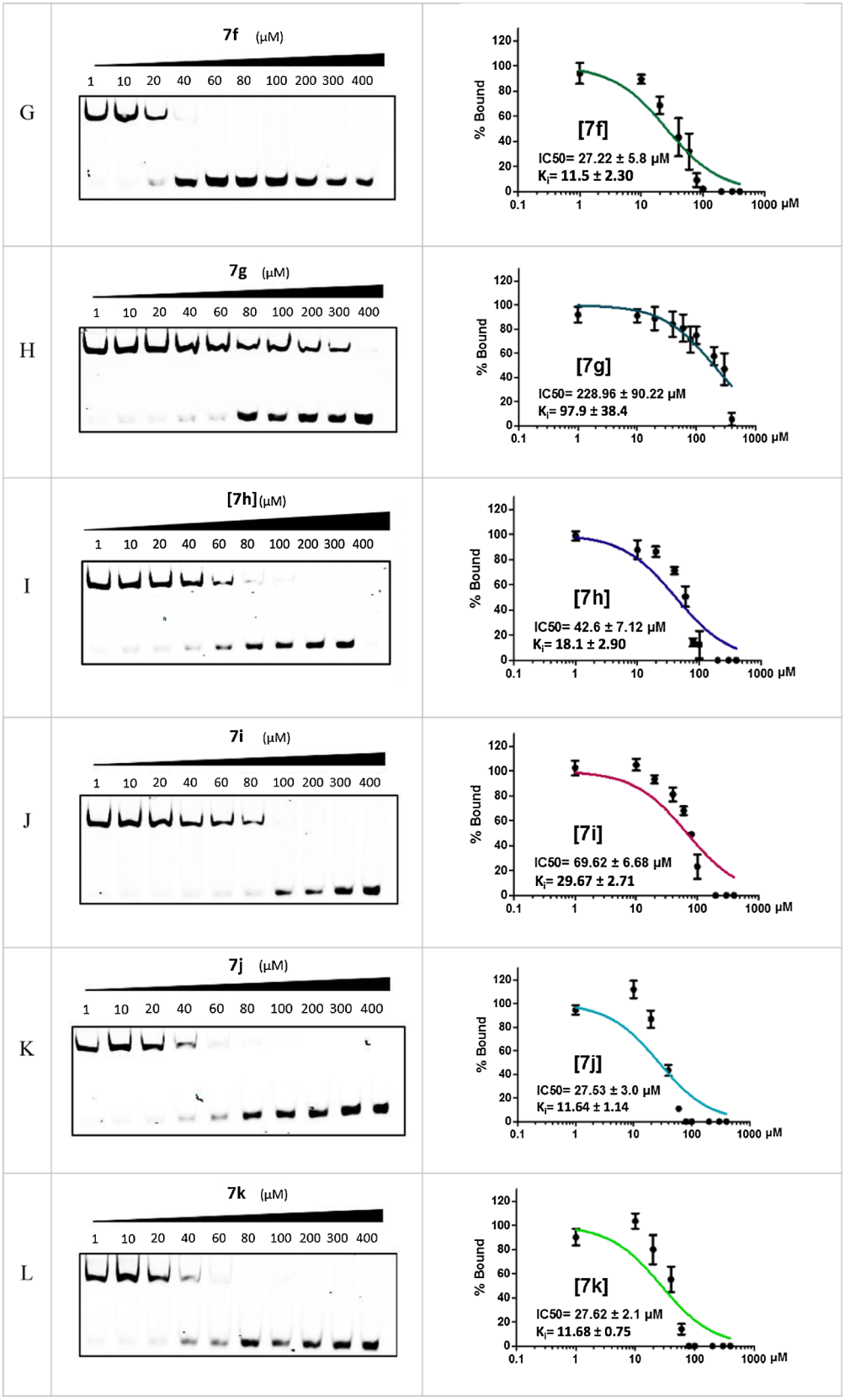

Fig. 4. (*continued*)

2.5. Molecular modeling

To further support the experimental observations suggesting the need for a halogen atom at the 4-position of the phenyl moiety of FDI drugs, we carried out a series of complementary docking and molecular dynamic simulations with compounds **7a**, **7b**, **7c**, **7g**, **7h**, **7i**, **7j** and **7k** comparing their binding profile with that of other molecules in the same series (Table 2). In this regard, we observed a direct relationship

Table 2
Free binding energies calculated for eight FDI derivatives. The total binding energies represent the sum of Van der waals, electrostatic, solvent accessible surface area (SASA), and polar solvation energy, during the last nanosecond of the corresponding molecular dynamic simulation.

Compound	Van Der Waal Energy (kJ/mol)	Electrostatic Energy (kJ/mol)	Polar Solvation Energy A (kJ/mol)	SASA Energy (kJ/mol)	Binding Energy (kJ/mol)	Binding Energy (kcal/mol)
7a	−89.7 ± 5.3	−14.7 ± 3.7	55.9 ± 35.3	−9.09 ± 1.1	−57.6 ± 38.1	−13.7 ± 9.1
7b	−94.8 ± 16.9	−7.7 ± 5.5	40.6 ± 16.6	−11.5 ± 1.9	−73.4 ± 11.5	−17.5 ± 2.7
7c (FDI-6)	−147.6 ± 16.2	−3.3 ± 2.9	59.0 ± 31.9	−13.7 ± 0.6	−105.6 ± 34.2	−25.2 ± 8.1
7g	−62.9 ± 41.6	0.5 ± 2.8	31.3 ± 31.6	−7.9 ± 5.1	−38.9 ± 44.7	−9.2 ± 10.6
7h	−122.4 ± 12.0	−3.1 ± 3.3	55.7 ± 19.5	−12.9 ± 0.8	−72.9 ± 24.8	−17.4 ± 5.9
7i	−69.2 ± 34.6	−4.8 ± 4.8	41.0 ± 18.3	−8.6 ± 4.3	−41.7 ± 30.9	−9.9 ± 7.3
7j	−5.7 ± 25.5	−0.8 ± 3.9	−3.5 ± 31.5	−0.9 ± 2.8	−11.0 ± 15.3	−2.6 ± 3.6
7k	−96.2 ± 14.8	−7.6 ± 6.2	40.5 ± 17.0	−11.6 ± 1.5	−74.8 ± 10.0	−17.8 ± 2.3

between the position of the halogen (fluorine) atom and the total binding energy calculated for the corresponding drug molecule: 4-flouro (−25.2 kcal/mol), 3-flouro, −17.4 kcal/mol, and 2-flouro (−9.9 kcal/mol). With these results, we think it is reasonable to propose that the strength of the binding force between the drug molecule and the FOXM1 protein is determined, at least in part, by the relative position of the fluorine atom, in which 4-phenyl > 3-phenyl > 2-phenyl. Compound **7c** (FDI-6) showed the strongest binding energy (−25.2 kcal/mol), with a low ligand Positional Root Media Square Deviation (RMSD), compared to compounds **7b** (phenyl), **7h** [3-(fluoro) phenyl], and **7i** [2-(fluoro)phenyl] (**Fig. S23**), Supplementary information). The low RMSD values observed for **7c**, along with the low Van Der Waal energy (VDW, −147.6 Kj/mol), suggests that the 4-(flouro)phenyl moiety increases the stability of a possible active conformation inside the binding pocket during the molecular dynamic simulation.

As shown in Table 2, with the exception of compound **7j** we could correlate the binding energies for all compounds with the screening assays described above. In other words, the unusually high theoretical binding energy (low binding force = −2.6 Kcal/mol) calculated for **7j**, would suggest a weak activity profile, but this was not the case. Compound **7j** decreased cell proliferation in MDA-MB-231 cells, it significantly decreased the FOXM1 protein level of FOXM1, and it showed significant activity in the EMSA.

Finally, in Fig. 5 we present a graphical representation of the binding conformations observed for compounds **7c** [4-(fluoro)phenyl] and **7h** [3-(fluoro)phenyl] and their relative distance from Arg297 in which we observed practically the same binding interactions between the drug molecules and the Arg297.

3. Summary and conclusions

We present a series of in vitro and in silico experiments supporting the essential role played by a 4-(halo)phenyl moiety in the chemical structure of FDIs involving an Arg297 amino acid residue within the DBD of the FOXM1 protein. Despite a few minor differences in the relative potency of individual compounds among individual assays, we propose that (1) the halogen binding interaction is equipotent for 4-fluoro, 4-chloro, 4-bromo, or 4-iodo groups; (2) a bioisosteric replacement involving a 4-(methyl)phenyl group (**7j**) did not result in significant binding interactions or an improved activity profile. However, the use of a 4-(trifluoromethyl)phenyl moiety is a suitable strategy to improve the potency of FDIs (by about two-fold) as shown in the EMSA, and it maintained the drug's cancer cell proliferation inhibitory profile in triple negative-breast cancer (MDA-MB-231) cells.

One major limitation associated with this work is the fact that we are not considering the effects produced by the test drugs on other (potential) targets that would affect cell proliferation or FOXM1 protein expression. However, the EMSA assay is relatively selective to evaluate the effects produced by "direct" FOXM1 inhibitors, distinguishing between inactive and active drugs that bind to (and interfere with) the

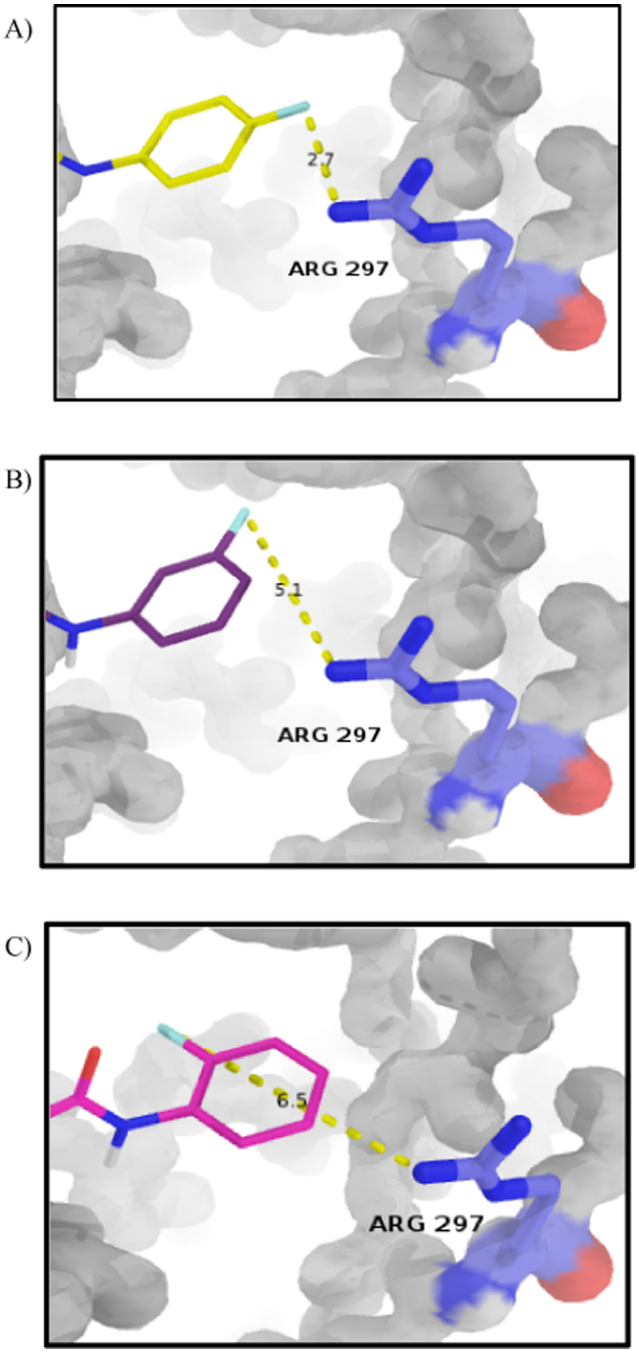

Fig. 5. The graphical representation of the relative distance [Å] of fluorine atom of **7c**, 2.7 Å (A), **7h**, 5.1 Å (B) and **7i**, 6.5 Å (C) to Arg297.

protein's DNA binding domain. In this regard, we used structurally unrelated molecules as negative controls (ranolazine and andrographolide) and we did not observe dissociation (at any drug concentration) of the protein-DNA complex (Fig. S25; supplementary information).

In summary, we provide evidence validating the essential role of a 4-(halo)phenyl–Arg297 binding interaction as part of the overall mechanism of action exerted by FDIs, postulated by our group, in a previous publication [15]. In this report, we also propose a specific binding interaction to fine-tune the design of FOXM1 inhibitors based on the chemical scaffold of the lead FDI-6 molecule first described by Gormally et al. [14] and we submit that this model could also be used in the design of small-molecule drugs possessing a 4-(halo)phenyl moiety.

4. Experimental section

4.1. General information

All the reagents and solvents were purchased from Sigma-Aldrich and were used without further purification. All reactions were monitored by thin-layer chromatography (RediSep® TLC plates) and visualized using UV light. Melting points were measured with an Electrothermal melting point apparatus (Thermofisher, USA) and were uncorrected. ^{1}H NMR and ^{13}C NMR spectra were determined on a Bruker FT-600 MHz instrument (600 MHz and 150 MHz, respectively) using DMSO-d_6 as the solvent and TMS as a reference. Chemical shifts (δ) and coupling constants (*J*) are expressed in parts per million and Hertz, respectively. Signal multiplicity is expressed as s (singlet), d (doublet), t (triplet), q (quartet), m (multiplet) and br (broad singlet). Elemental analyses were performed on a Carlo Erba EA1108 Elemental Analyzer and the results are within ± 0.4% of the theoretical values. The synthesis of 6-(thiophen-2-yl)-2-thioxo-4-(trifluoromethyl)-1,2-dihydropyridine-3-carbonitrile (3) was carried out following the method reported [19], and confirmed by ^{1}H, ^{13}C and ^{19}F NMR. 2-Chloroacetamide (**6a**) was purchased from Sigma Aldrich; compounds **6b-6k** were synthesized based on protocols previously reported [22–24] and confirmed by ^{1}H NMR (more details in the supplementary information). FDI derivatives **7a-7c**, and **7f**, were confirmed by ^{1}H and ^{13}C spectra, both in agreement to those reported in literature [19] (see supporting information, Figs. S1-S22). The microwave-assisted synthesis of derivatives **7a-7k** was carried out using a Biotage Initiator Reactor. All test compounds were purified by flash column chromatography using a Combi Flash EZ prep (Teledyne isco), using prepacked silica cartridges (RediSep Rf® Gold Resolution) and a gradient of hexane-ethyl acetate as mobile phase.

4.2. General procedure for synthesis of compounds *7a-7k*

The corresponding chloroacetamide **6a-6 k** (1 equiv.), compound **3** (suppl. info.; 1 equiv.) was mixed with K_2CO_3 (1 equiv.), and ethanol (5 mL) in a microwave reaction vessel. This mixture was stirred at 90 °C for 2 h using a "high energy absorption" setting. The crude product was filtered-off, washed with water and fixed onto silica gel powder before running a solvent gradient (flash column chromatography). Combined organic fractions were dried under vacuum and the corresponding final product was recrystallized from ethanol (when needed).

4.2.1. 3-Amino-N-(4-bromophenyl)-6-(thiophen-2-yl)-4-(trifluoromethyl) thieno[2,3-b]pyridine-2-carboxamide (*7d*)

6d (65 mg, 0.22 mmol), **3** (63 mg, 0.22 mmol) and K_2CO_3 (30 mg, 0.22 mmol) in 5 mL of ethanol, yellow (flocculent) crystals, 90% yield (100 mg, 0.2 mmol), mp: 225–227 °C; ^{1}H NMR (600 MHz, DMSO-d_6) δ 9.78 (s, 1H), 8.33 (s, 1H), 8.25 (dd, *J* = 3.8, 1.1 Hz, 1H), 7.89 (dd, *J* = 5.0, 1.1 Hz, 1H), 7.75–7.68 (m, 2H), 7.56–7.51 (m, 2H), 7.32 (dd, *J* = 5.0, 3.7 Hz, 1H), 6.91 (s, 2H). ^{13}C NMR (151 MHz, DMSO-d_6) δ 131.55, 131.38, 129.49, 129.23, 124.26, 40.52, 40.24. 13C NMR (151 MHz, DMSO) δ 164.49, 160.99, 152.15, 142.72, 132.16, 131.91, 131.55, 131.38, 129.49, 129.23, 125.93, 124.26, 124.12, 122.30, 120.49, 118.74, 112.86, 112.82. Anal. Calc. for (%) $C_{19}H_{11}BrF_3N_3OS_2$, C 45.79; H 2.23, N 8.43; S 12.87; found C 45.72, H 2.44, N 8.10, S 12.51.

4.2.2. 3-Amino-N-(4-iodophenyl)-6-(thiophen-2-yl)-4-(trifluoromethyl) thieno[2,3-b]pyridine-2-carboxamide (*7e*)

6e (55 mg, 0.18 mmol), **3** (54 mg, 0.18 mmol) and K_2CO_3 (25 mg, 0.18 mmol) in 5 mL of ethanol, yellow (flocculent) crystals, 92% yield (90 mg, 0.19 mmol); mp: 226–228 °C;^{1}H NMR (600 MHz, DMSO-d_6) δ 9.87 (s, 1H), 8.35 (s, 1H), 8.28 (dd, *J* = 3.8, 1.1 Hz, 1H), 7.91 (dd, *J* = 5.0, 1.1 Hz, 1H), 7.77–7.71 (m, 2H), 7.63–7.57 (m, 2H), 7.32 (dd, *J* = 5.0, 3.7 Hz, 1H), 6.85 (s, 2H). ^{13}C NMR (151 MHz, DMSO-d_6) δ 164.09, 161.04, 152.78, 145.55, 142.54, 137.59, 132.47, 132.25, 131.67, 129.57, 129.54, 125.84, 124.12, 122.21, 118.27, 113.16, 113.12, 88.03. Anal. Calc. for (%) $C_{19}H_{11}F_3IN_3OS_2$, C 41.85, H 2.03, N 7.71, S 11.76; found C 41.31, H 2.10, N 7.45, S 11.69.

4.2.3. 3-Amino-N-(4-methylphenyl)-6-(thiophen-2-yl)-4-(trifluoromethyl) thieno[2,3-b]pyridine-2-carboxamide (*7g*)

6 g (40 mg, 0.2 mmol), **3** (60 mg, 0.2 mmol) and K_2CO_3 (30 mg, 0.18 mmol) in 5 mL of Ethanol, yellow (flocculent) crystals yellow powder, 90% yield (80 mg, 0.18 mmol), mp: 233–235 °C;^{1}H NMR (600 MHz, DMSO-d_6) δ 9.69 (s, 1H), 8.31 (s, 1H), 8.23 (dd, *J* = 3.8, 1.1 Hz, 1H), 7.86 (dd, *J* = 5.0, 1.1 Hz, 1H), 7.58–7.53 (m, 2H), 7.28 (dd, *J* = 5.0, 3.8 Hz, 1H), 7.19–7.15 (m, 2H), 6.75 (s, 2H), 2.30 (s, 3H). ^{13}C NMR (151 MHz, DMSO-d_6) δ 163.91, 160.95, 152.70, 145.33, 142.56, 136.31, 133.53, 132.46, 132.24, 131.64, 129.54, 129.38, 124.04, 122.21, 118.37, 113.15, 113.11, 101.61, 20.99. Anal. Calc. for (%) $C_{20}H_{14}F_3N_3OS_2$, C 55.42, H 3.26, N 9.69, S 14.79, found C 55.42, H 3.31, N 9.49, S 15.08

4.2.4. 3-Amino-N-(3-fluorophenyl)-6-(thiophen-2-yl)-4-(trifluoromethyl) thieno[2,3-b]pyridine-2-carboxamide (*7h*)

6 h (45 mg, 0.23 mmol), **3** (65 mg, 0.23 mmol) and K_2CO_3 (30 mg, 0.23 mmol) in 5 mL of ethanol, yellow (flocculent) crystals yellow powder, 92% yield (90 mg, 0.21 mmol), mp: 218–220 °C; ^{1}H NMR (600 MHz, DMSO-d_6) δ 9.95 (s, 1H), 8.35 (s, 1H), 8.27 (dd, *J* = 3.8, 1.1 Hz, 1H), 7.90 (dd, *J* = 5.0, 1.1 Hz, 1H), 7.71 (ddd, *J* = 11.8, 2.6, 1.9 Hz, 1H), 7.57 (ddd, *J* = 8.2, 1.9, 0.9 Hz, 1H), 7.44 (td, *J* = 8.2, 6.9 Hz, 1H), 7.32 (dd, *J* = 5.0, 3.7 Hz, 1H), 6.99 (tdd, *J* = 8.5, 2.6, 0.9 Hz, 1H), 6.87 (s, 2H). ^{13}C NMR (151 MHz, DMSO): δ 164.21, 163.21, 161.61, 161.07, 152.91, 145.83, 142.50, 140.95, 132.53, 132.31, 131.72, 130.54, 130.48, 129.63, 129.55, 125.83, 124.02, 122.20, 118.18, 117.49, 117.48, 113.20, 113.16, 110.76, 110.62, 108.56, 108.39, Anal. Calc. for (%) $C_{19}H_{11}F_4N_3OS_2$, C 52.17, H 2.53, N 9.61, S 14.66 found C 51.80, H 2.63, N 9.28, S 14.88.

4.2.5. 3-Amino-N-(2-fluorophenyl)-6-(thiophen-2-yl)-4-(trifluoromethyl) thieno[2,3-b]pyridine-2-carboxamide (*7i*)

6i (45 mg, 0.23 mmol), **3** (65 mg, 0.23 mmol) and K_2CO_3 (30 mg, 0.23 mmol) in 5 mL of ethanol, yellow (flocculent) crystals, 95% yield (93 mg, 0.22 mmol); mp: 248–250 °C;^{1}H NMR (600 MHz, DMSO-d_6) δ 9.73 (s, 1H), 8.32 (s, 1H), 8.24 (dd, *J* = 3.8, 1.1 Hz, 1H), 7.86 (dd, *J* = 5.0, 1.1 Hz, 1H), 7.51 (t, *J* = 7.8 Hz, 1H), 7.36–7.29 (m, 2H), 7.28 (dd, *J* = 5.0, 3.7 Hz, 1H), 7.27–7.20 (m, 1H), 6.76 (s, 2H). ^{13}C NMR (151 MHz, DMSO-d_6) δ 164.08, 161.10, 157.77, 156.13, 152.87, 145.57, 142.53, 132.61, 132.39, 131.72, 129.64, 129.56, 128.47, 127.97, 127.92, 125.74, 125.66, 124.78, 124.00, 122.19, 118.29, 116.38, 116.25, 113.19, 113.15, 100.96. Anal. Calc. for (%) $C_{19}H_{11}F_4N_3OS_2$ C 52.17, H 2.53, N 9.61, S 14.66 found C 52.19, H 2.71, N 9.36, S 15.02.

4.2.6. 3-Amino-6-(thiophen-2-yl)-4-(trifluoromethyl)-N-[4(trifluoromethyl)phenyl]thieno[2,3-b]pyridine-2-carboxamide (7j)

6j (55 mg, 0.22 mmol), **3** (65 mg, 0.22 mmol) and K_2CO_3 (30 mg, 0.22 mmol) in 5 mL of ethanol, yellow (flocculent) crystals, 95% yield (100 mg, 0.21 mmol), mp: 183–185 °C; ^{1}H NMR (600 MHz, DMSO-d_6) δ 10.05 (s, 1H), 8.30 (s, 1H), 8.23 (dd, J = 3.8, 1.1 Hz, 1H), 7.94 (d, J = 8.5 Hz, 2H), 7.86 (dd, J = 5.0, 1.1 Hz, 1H), 7.70 (d, J = 8.5 Hz, 2H), 7.27 (dd, J = 5.0, 3.7 Hz, 1H), 6.86 (s, 2H): ^{13}C NMR (151 MHz, DMSO-d_6) δ 164.52, 161.14, 152.85, 142.54, 132.50, 132.28, 131.70, 129.60, 129.54, 127.62, 126.15, 126.13, 126.10, 125.82, 124.03, 122.22, 121.65, 121.63, 120.40, 118.22, 113.16, 113.12. Anal. Calc. for (%) $C_{20}H_{11}F_6N_3OS_2$ C 49.28, H 2.27, N 8.62, S 13.15 found C 49.09, H 2.30, N 8.33, S 12.93.

4.2.7. 3-Amino-N-(3,5-difluorophenyl)-6-(thiophen-2-yl)-4-(trifluoromethyl)thieno[2,3-b]pyridine-2-carboxamide (7k)

6 k (50 mg, 0.23 mmol), **3** (65 mg, 0.23 mmol) and K_2CO_3 (35 mg, 0.23 mmol) in 5 mL of ethanol, red needle crystals, 95% yield (100 mg, 0.22 mmol), mp: 208–210 °C; ^{1}H NMR (600 MHz, DMSO-d_6) δ 10.02 (s, 1H), 8.30 (s, 1H), 8.23 (dd, J = 3.8, 1.1 Hz, 1H), 7.86 (dd, J = 5.0, 1.1 Hz, 1H), 7.54–7.46 (m, 2H), 7.27 (dd, J = 5.0, 3.7 Hz, 1H), 6.92 (t, J = 9.3 Hz, 1H), 6.86 (s, 2H). ^{13}C NMR (151 MHz, DMSO-d_6) δ 163.53, 163.43, 161.92, 161.82, 161.15, 153.15, 148.79, 146.32, 146.31, 132.64, 132.42, 132.03, 131.85, 129.92, 129.77, 129.57, 125.80, 123.99, 122.17, 118.02, 113.30, 113.26, 104.31, 104.27, 104.15, 104.11, 99.37, 99.20, 99.03. Anal. Calc. for (%) $C_{19}H_{10}F_5N_3OS_2$ C 50.11, H 2.21, N 9.23, S 14.08 found C 49.78, H 2.39, N 8.91, S 13.66.

4.3. Cell culture

The MDA-MB-231 and MCF-7 cells were a generous gift from Dr. Frank Wuest (Cross Cancer Institute; Edmonton, Alberta, Canada). The cells were cultured in RPMI and DMEM media respectively, supplemented with 10% fetal bovine serum (FBS) in a 5% CO_2 atmosphere at 37 °C.

4.4. Cell proliferation inhibition (MTT) assay

Cells were seeded in 96-well plates (approx. 4000 cells/well for MDA-MB-231 and approx. 5000 for MCF-7), then we added the test compounds at different concentrations and we incubated all plates for 72 h. We added 30 µL of MTT solution (3 mg/ml) and continued the incubation for 3 h at 37 °C. The precipitate crystals were dissolved using DMSO, and the absorbance of the resulting solution was recorded at 570 nm using a Synergy H1-Hybrid Multi-Mode Reader (BioTek). We analyzed the data using GraphPad Prism. All experiments were carried out in triplicate.

4.5. Antibodies

We used a FOXM1 mouse monoclonal antibody (Santa Cruz Biotechnology) and IRDye® 800CW Goat anti-Mouse IgM (Li-Cor Biosciences).

4.6. Western blot

After treatment with test compounds for 24 h at different concentrations, the cells were trypsinized; the FOXM1 protein was isolated with RIPA lysis and extraction buffer (Thermo fisher) according to the manufacturer's protocol. The protein levels in the supernatant were measured using the Bradford assay. Then the protein (40 µg/lane) was loaded into a 4–20% SDS-PAGE (Sodium dodecyl sulfate Polyacrylamide gel electrophoresis). After completion of the run, the protein was transferred from the gel to a nitrocellulose membrane (Thermofisher), and stained with REVERT (Li-Cor Biosciences) total protein stain. The membrane was then detected in the 700 nm channel using Odyssey scanner (LI-COR Biosciences). The REVERT was then reversed and the membrane was blocked with 10% fat-free milk in TBST for 1 h. The membrane was incubated with the primary antibody (1:1000 dilution) at 4 °C overnight. Then, the membrane was washed three times with TBST, incubated with the corresponding Li-Cor secondary antibody and incubated again at room temperature for 1 h. The membrane was washed three times (15 min total) with TBST. The blots were visualized using Odyssey scanner (LI-COR Biosciences). The quantification was carried out for all proteins relative to total protein (REVERT) using ImageJ for each lane.

4.7. Protein expression and purification

We used the PEX-*N*-GST-FOXM1-DBD plasmid (OriGene Technologies, USA) transformed into BL21(DE3) E. Coli cells; positive colonies were selected on LB agar plates with ampicillin (100 µg/mL). Then, these cells were grown in LB media with ampicillin (100 µg/ml) at 37 °C with orbital shaking at 220 rpm until reaching an optical density (OD600) of 0.8; protein expression was induced by adding 1 mM isopropyl β-D-1-thiogalactopyranoside (IPTG) for 6 hr at 37 °C. The GST protein and GST-FOXM1 protein from soluble fractions were purified using glutathione resin (GenScript, USA), following the manufacturer's instructions. Please see **Fig. S24** for the representative gel image of purified protein.

4.8. Electromobility shift assay

All values of a titration (binding) curve of recombinant FOXM1-DBD with its target double strand DNA oligo (Forward strand: 5′-/IRD700/-AAACAAACAAACAATCAAACAAACAAACAATC-3′), were recorded using EMSA by the method previously reported by Gormally et al. [14] Briefly, dsDNA and an increasing concentration of the FOXM1 protein were incubated at RT for 30 min in a buffer solution containing 20 mM Tris (pH 7.5), 100 mM KCl, 1 mM EDTA, 0.1 mM DTT, and 10% glycerol, before running the samples on 6% native gel for 30 min at 120 V. The dissociation constant of protein DNA complex (K_d) was calculated using Graph pad Prism 6.2. The displacement EMSA experiments were carried out by incubating each test compound with the recombinant FOXM1-DBD protein, for 1.5 h, at room temperature, followed by a second incubation with DNA, for 20 min, before conducting the electrophoresis. The concentration of FOXM1-DBD and DNA in each reaction was 480 nM and 12.8 nM, respectively. The K_i values were calculated for each compound (**7a-7k**) using Eq. (1) [25]:

$$Ki = \frac{[I]_{50}}{\left(\frac{([I]_{50})}{K_d} + \frac{[P]_0}{K_d} + 1\right)} \quad (1)$$

where $[I]_{50}$ = IC_{50} of the inhibitor; $[L]_{50}$ = concentration of IR-labelled DNA at 50% inhibition; [P] = concentration of the FOXM1 protein; and K_d = dissociation constant calculated from the initial titration curve.

4.9. Molecular modeling and dynamics simulations

The crystal structure of FOXM1-DBD was acquired from the protein data bank (PDB_ID: 3G73) [11]. Using Pymol v.1.8 [26], we removed Chain A followed by a short minimization using CHIMERA V 1.10.2 [27], the missing sidechains were added and the protonated group was equilibrated to the biological pH 7.0 using PROPKA [28].

All the 3D format structures were prepared for docking using the dock prep tool of UCSF CHIMERA V1.10.2 in the framework of AMBER99SB force field. All the compounds were docked in a previously identified binding pocket [15], into a grid of 40 × 40 × 50 Å with a spacing of 0.375 Å using Autodock vina [29]; 12 runs per docking were performed with the exhaustiveness of 40 for each ligand. Before performing the molecular dynamic simulation on the Protein-ligand complexes, we performed a molecular dynamic simulation on the FOXM1-

DBD using GROMACS 4.5.6 package [30]. We used the TIP3P water models to solvate the protein with 1 nm marginal cushion on each side. The box was then neutralized using NaCl, and the system was minimized using the AMBER99SB0ILDN force field. The system was heated to 300 K and equilibrated for 500 ps using the Berendsen Thermostat. Using the Isothermal-isobaric ensemble at 1 bar with the Parrinello-Rahman barostat an additional equilibration was also performed. A 20 ns production run was performed using the periodic boundary condition. The Lenard-Jones, the Coulomb (Cut-off = 1.0 nm), and the Particle Mesh Ewald (PME) were used to calculate the VDW and electrostatic interactions. The FOXM1-DBD/Ligand complexes were performed using the same condition. The AnteChamber Python Parser interfacE (ACPYPE) [31] was used for ligand parameterization. The Root Mean Square Deviation (RMSD), Root Mean Square Fluctuation (RMSF) and ligand positional RMSD were calculated using GROMACS tools. All the data were plotted using the GraphPad Prism 6.0.7. Discovery Studio Visualizer [32] and the Schrodinger's PyMOL package were used as the visualization tools.

The free energy of interaction between each ligand and FOXM1-DBD was calculated using the g_mmpbsa Gromacs tool [33]. Using the Molecular Mechanic Poisson-Boltzmann Surface Area (MM-PBSA), this program calculates the binding free energy based on the electrostatic and VDW interactions besides polar and non-polar solvation energies. The G_mmpbsa module solves the following Eqs. (2) and (3) to calculate the binding energy of ligands:

$$\Delta G_{bidning} = G_{complex} - (G_{protein} + G_{ligand}) \quad (2)$$

where the $G_{complex}$ is the protein-ligand complex total free energy, $G_{protein}$ is the total free energy of protein and G_{ligand} is the total energy of ligand in solvent. The free energy of protein ligand complex, isolated protein and isolated ligand (G) can be given by:

$$G = E_{MM} - TS + G_{solvation} \quad (3)$$

where E_{MM} is the average of molecular mechanics potential in vacuum, $TS$is the Temprature and Entropy respectively and $G_{solvation}$ is the solvation free energy [33].

Declaration of Competing Interest

The authors declare no competing financial interest.

Acknowledgments

Authors acknowledge the support from the Noujaim Fund for Strategic Initiatives, Faculty of Pharmacy and Pharmaceutical Sciences, University of Alberta. A portion of the described studies were also supported from a Discovery Grant (RGPIN-2015-04946) from the Natural Sciences and Engineering Research Council of Canada to J.R.U; S.A.T.D is the recipient of Antoine Noujaim graduate scholarship. This research was enabled in part by Compute Canada and its regional partner WestGrid. D.J.P is grateful for the Postdoctoral Fellowship (287012) granted by the National Council for Science and Technology (CONACYT, Mexico).

Appendix A. Supplementary material

General procedure for the synthesis of compounds **6b-6k** and **3**, NMR spectra for compounds **7a-7k** (Figs. S1–S21), the ligand positional RMSD calculated for compounds **7b**, **7c**, **7h** and **7i** (Fig. S23), and a representative gel image of the purified GST-FOXM1-DBD (Fig. S24). Supplementary data to this article can be found online at https://doi.org/10.1016/j.bioorg.2019.103269.

References

[1] W. Korver, J. Roose, A. Wilson, H. Clevers, The Winged-Helix transcription factor trident is expressed in actively dividing lymphocytes, Immunobiology 198 (1997) 157–161.
[2] K.-M. Yao, M. Sha, Z. Lu, G.G. Wong, Molecular Analysis of a Novel Winged Helix Protein, win: expression pattern, DNA binding property, and alternative splicing within the DNA binding domain, J. Biol. Chem. 272 (1997) 19827–19836.
[3] H. Ye, T.F. Kelly, U. Samadani, L. Lim, S. Rubio, D.G. Overdier, K.A. Roebuck, R.H. Costa, Hepatocyte nuclear factor 3/fork head homolog 11 is expressed in proliferating epithelial and mesenchymal cells of embryonic and adult tissues, Mol. Cell. Biol. 17 (1997) 1626–1641.
[4] M.-T. Teh, E. Gemenetzidis, T. Chaplin, B.D. Young, M.P. Philpott, Upregulation of FOXM1 induces genomic instability in human epidermal keratinocytes, Mol. Cancer 9 (2010) 45.
[5] Z. Wang, A. Ahmad, Y. Li, S. Banerjee, D. Kong, F.H. Sarkar, Forkhead box M1 transcription factor: A novel target for cancer therapy, Cancer Treat. Rev. 36 (2010) 151–156.
[6] H. Chen, Y. Zou, H. Yang, J. Wang, H. Pan, Downregulation of FoxM1 inhibits proliferation, invasion and angiogenesis of HeLa cells in vitro and in vivo. International Journal of Oncology, Int. J. Oncol. 45 (2014) 2355–2364.
[7] Y. Zhang, N. Zhang, B. Dai, M. Liu, R. Sawaya, K. Xie, S. Huang, FoxM1B transcriptionally regulates vascular endothelial growth factor expression and promotes the angiogenesis and growth of glioma cells, Cancer Res. 68 (2008) 8733–8742.
[8] B.Y. Fei, X. He, Jie Ma, M. Zhang, R. Chai, FoxM1 is associated with metastasis in colorectal cancer through induction of the epithelial-mesenchymal transition, Oncol Lett. 14 (2017) 6553–6561.
[9] A. Bergamaschi, Z. Madak-Erdogan, Y.J. Kim, Y.-L. Choi, H. Lu, B.S. Katzenellenbogen, The forkhead transcription factor FOXM1 promotes endocrine resistance and invasiveness in estrogen receptor-positive breast cancer by expansion of stem-like cancer cells, Breast Cancer Res. 16 (2014) 436.
[10] X. Song, S.S. Fiati Kenston, J. Zhao, D. Yang, Y. Gu, Roles of FoxM1 in cell regulation and breast cancer targeting therapy, Med. Oncol. 34 (2017) 41.
[11] D.R. Littler, M. Alvarez-Fernández, A. Stein, R.G. Hibbert, T. Heidebrecht, P. Aloy, R.H. Medema, A. Perrakis, Structure of the FoxM1 DNA-recognition domain bound to a promoter sequence, Nucleic Acids Res. 38 (2010) 4527–4538.
[12] F. Fontaine, J. Overman, M. François, Pharmacological manipulation of transcription factor protein-protein interactions: opportunities and obstacles, Cell Regener. 4 (4) (2015) 2.
[13] A.M. Redmond, J.S. Carroll, Defining and targeting transcription factors in cancer, Genome Biol. 10 (2009) 311.
[14] M.V. Gormally, T.S. Dexheimer, G. Marsico, D.A. Sanders, C. Lowe, D. Matak-Vinković, S. Michael, A. Jadhav, G. Rai, D.J. Maloney, A. Simeonov, S. Balasubramanian, Suppression of the FOXM1 transcriptional programme via novel small molecule inhibition, Nat. Commun. 5 (2014) 5165.
[15] S.A. Tabatabaei-Dakhili, R. Aguayo-Ortiz, L. Domínguez, C.A. Velázquez-Martínez, Untying the knot of transcription factor druggability: Molecular modeling study of FOXM1 inhibitors, J. Mol. Graphics Modell. 80 (2018) 197–210.
[16] N.S. Hegde, D.A. Sanders, R.L. Rodriguez, S. Balasubramanian, The transcription factor FOXM1 is a cellular target of the natural product thiostrepton, Nat. Chem. 3 (2011) 725–731.
[17] A.L. Gartel, Thiostrepton, proteasome inhibitors and FOXM1, Cell Cycle 10 (2011) 4341–4342.
[18] V. Petrovic, R.H. Costa, L.F. Lau, P. Raychaudhuri, A. Tyner, Negative regulation of the oncogenic transcription factor FoxM1 by thiazolidinediones and mithramycin, Cancer Biol. Ther. 9 (2010) 1008–1016.
[19] M.I. Abdel-Monem, O.S. Mohamed, E.A. Bakhite, Fluorine-containing heterocycles: Synthesis and some reactions of new 3-amino-2-functionalized-6-(2′-thienyl)-4-trifluoromethylthieno [2,3-b]pyridines, Pharmazie 56 (2001) 41–44.
[20] G.A. Patani, E.J. LaVoie, Bioisosterism: a rational approach in drug design, Chem. Rev. 96 (1996) 3147–3176.
[21] A.L. Gartel, Targeting FOXM1 auto-regulation in cancer, Cancer Biol. Ther. 16 (2015) 185–186.
[22] M.A. Matulenko, A.A. Hakeem, T. Kolasa, M. Nakane, M.A. Terranova, M.E. Uchic, L.N. Miller, R. Chang, D.L. Donnelly-Roberts, M.T. Namovic, R.B. Moreland, J.D. Brioni, A.O. Stewart, Synthesis and functional activity of (2-aryl-1-piperazinyl)-N-(3-methylphenyl)acetamides: selective dopamine D4 receptor agonists, Bioorg. Med. Chem. 12 (2004) 3471–3483.
[23] R.V. Patel, P.K. Patel, P. Kumari, D.P. Rajani, K.H. Chikhalia, Synthesis of benzimidazolyl-1,3,4-oxadiazol-2ylthio-N-phenyl (benzothiazolyl) acetamides as antibacterial, antifungal and antituberculosis agents, Eur. J. Med. Chem. 53 (2012) 41–51.
[24] W. Zhang, J. Ai, D. Shi, X. Peng, Y. Ji, J. Liu, M. Geng, Y. Li, Discovery of novel type II c-Met inhibitors based on BMS-777607, Eur. J. Med. Chem. 80 (2014) 254–266.
[25] Z. Nikolovska-Coleska, R. Wang, X. Fang, H. Pan, Y. Tomita, P. Li, P.P. Roller, K. Krajewski, N.G. Saito, J.A. Stuckey, S. Wang, Development and optimization of a binding assay for the XIAP BIR3 domain using fluorescence polarization, Anal. Biochem. 332 (2004) 261–273.
[26] Schrödinger; LLC. The {PyMOL} Molecular Graphics System, Version 1.8, 2015.
[27] E.F. Pettersen, T.D. Goddard, C.C. Huang, G.S. Couch, D.M. Greenblatt, E.C. Meng, T.E. Ferrin, UCSF Chimera—A visualization system for exploratory research and analysis, J. Comput. Chem. 25 (2004) 1605–1612.
[28] C.R. Søndergaard, M.H.M. Olsson, M. Rostkowski, J.H. Jensen, Improved treatment of ligands and coupling effects in empirical calculation and rationalization of pKa values, J. Chem. Theory Comput. 7 (2011) 2284–2295.
[29] O. Trott, A.J. Olson, AutoDock Vina: Improving the speed and accuracy of docking with a new scoring function, efficient optimization, and multithreading, J. Comput. Chem. 31 (2010) 455–461.
[30] M.J. Abraham, T. Murtola, R. Schulz, S. Páll, J.C. Smith, B. Hess, E. Lindahl, GROMACS: High performance molecular simulations through multi-level parallelism from laptops to supercomputers, SoftwareX 1–2 (2015) 19–25.
[31] A.W. Sousa da Silva, W.F. Vranken, ACPYPE - AnteChamber PYthon Parser interfacE. *BMC Res*, Notes 5 (2012) 367.
[32] D. Systèmes, BIOVIA Discovery Studio Modeling Environment, 2015.
[33] R. Kumari, R. Kumar, A. Lynn, g_mmpbsa – GROMACS Tool for High-Throughput MM-PBSA Calculations, J. Chem. Inf. Model. 54 (2014) 1951–1962.